

Feasibility of multi-centric fMRI connectivity studies of Alzheimer's disease

Christian Dansereau^{a,b}, Celine Risterucci^c, Emilio Merlo Pich^c,
Douglas Arnold^d, Pierre Bellec^{a,b,*}

^a*Centre de Recherche de l'Institut Universitaire de Gériatrie de Montréal, Montréal, CA*

^b*Département d'Informatique et de recherche opérationnelle, Université de Montréal,
Montréal, CA*

^c*F. Hoffmann-La Roche Ltd., Basel, Switzerland*

^d*NeuroRx, Montreal, Quebec, Canada*

Abstract

Keywords: fmri, general linear model, effect size, multiple comparison, multisite, clinical trial analysis

Highlights

- etc

1. Introduction

Resting-state (RS) connectivity in fMRI is a promising biomarker for a variety of neurological diseases. Typically, in a clinical trial, a large cohort is recruited and evaluated at multiple sites spread over countries or even continents. The main potential issue with that approach is the lack of consistency in the multi-site RS connectivity acquisitions that may obscure clinically relevant information. Therefore the aims of the study were to: (1) characterize the amplitude of the site bias, i.e. the systematic differences in rs-fMRI connectivity across different acquisition sites; (2) Quantify the impact of the between-site variance on the power of statistical tests in resting-state fMRI.

The number of Canadians suffering from Alzheimer's disease (AD) is rapidly increasing, with tremendous social and economic impact. Despite the emergence of promising drugs, the recent clinical trials with demented patients have failed. Dementia however comes very late in the development of the disease, at a stage where the degeneration of neural tissues has likely gone beyond repair. In order to be efficient, therapies should be initiated in the decades predating dementia, in a preclinical stage where patients experience no or very mild symptoms (see

*Corresponding author

Email address: pierre.bellec@criugm.qc.ca (Pierre Bellec)

chapter 1.1). There are unfortunately no biomarker(s) that are currently predictive of AD in this preclinical stage, and could help identify the individuals that could benefit from such interventions. A promising technique is resting-state functional magnetic resonance imaging (rs-fMRI), which may be able to capture the early synaptic dysfunction seen in AD (see chapter 1.2). In order to be able to apply statistical analysis and machine learning methods we need to preprocess the data to remove as much as possible the effect of various artefacts (hardware and physiological). The preprocessing reduces the variability of the data and therefore provides more relevant and discriminative features (see chapter 1.3). In order to further improve the statistical power of there analysis, multiple academic groups are collaborating to pool their dataset to increase the sample size of the study. Unfortunately the gain in sample size comes with a new source of variability introduced by the multicentric acquisition. Site-specific MRI set-ups may bias the fMRI measures, and I am thus developing procedures for inter-site normalization. Account for these sources of variance are important since they may bias the predictive potential of rs-functional connectivity in a multi-site, in line with this last assumption we want to quantify the robustness of the feature selection and classifier to multi-site acquisition (see chapter 1.4).

In most experiments conducted in neuroimaging, the main factors that influence power are: (1) the size of the effect, determined by the difference of the mean connectivity of one group versus a control group and the variability of this difference across subjects and groups; and (2) the sample size, i.e. the number of subjects in the study (Desmond and Glover, 2002). This last factor is usually the only one controlled by the investigator, hence why an increasing number of researchers share multicentric, sometimes multiprotocol, data suitable to statistical analysis. In research it is very difficult to obtain a grant large enough to scan a cohort larger than 80 subjects, therefore researcher and consortium initiatives have started to pool their resources together to make initiative composed of publicly available large cohorts of subjects like the 1000 functional connectome (Biswal et al., 2010), ADNI (Mueller et al., 2005), among others. In clinical trial the justification for multicentric acquisition is more of a logistical one then a financial reason; they need to recruit a large amount of subject in a short period of time. In order to achieve this goal they mandate the recruitment to multiple clinical centers across the globe which accelerate the evaluation time of a drug. Although these centers may be similar by their scanner protocols, scanners will have difference in their software version, specific add-on to the scanners, and, most importantly, vendors (even field strength may differ in some cases). Unfortunately between studies, MR acquisition methodologies are among the most commonly cited sources of measurement variation (Friedman et al., 2006). This is why it is important to assess if multi-site resting-state connectivity analysis are feasible (we can combine the data from multiple sources while introducing a reasonable amount of variance which is still acceptable to detect effects in the data) and what corrective measure on the data should be applied to reduce the bias introduced by multi-site analysis. Among the factor of variability across sites, we can list the following 3 categories described in (Yan et al., 2013b):

1. *Acquisition-related variations:*
 - (a) *Scanner make and model* (Friedman et al., 2006)
 - (b) *Sequence type* (*spiral vs. echo planar; single-echo vs. multi-echo*) (Klarhofer et al., 2002), *parallel vs. conventional acquisition* (Feinberg et al., 2010) (Lin et al., 2005)
 - (c) *Coil type* (*surface vs. volume, number of channels, orientation*).
 - (d) *Acquisition parameters: repetition time, number of repetitions, flip angle, echo time, and acquisition volume* (*field of view, voxel size, slice thickness/gaps, slice prescription*) (Friedman and Glover, 2006).
2. *Experimental-related variations:*
 - (a) *Participant instructions* (Hartstra et al., 2011), *eyes-open/eyes-closed* (Yan et al., 2009) (Yang et al., 2007), *visual displays, experiment duration* (Fang et al., 2007) (Van Dijk et al., 2010).
3. *Environment-related variations:*
 - (a) *Sound attenuation measures* (Cho et al., 1998) (Elliott et al., 1999).
 - (b) *Attempts to improve participant comfort during scans* (*e.g., music, videos*) (Cullen et al., 2009).
 - (c) *Head-motion restraint techniques* (*e.g., vacuum pad, foam pad, bite-bar, plaster cast head holder*) (Edward et al., 2000) (Menon et al., 1997).
 - (d) *Room temperature and moisture* (Vanhoutte et al., 2006).

In 2009, the publicly released 1000 Functional Connectomes Project (FCP) and International Neuroimaging Data-sharing Initiative (INDI) provided a glimpse of the variability in imaging methodologies employed by the neuroimaging field. The dataset includes rs-fMRI samples independently collected at imaging sites around the world. A noteworthy aspect of this dataset is the variation in almost every parameter of the imaging acquisition methodologies, while the majority of subject-related variables are not reported (due in most cases, to the fact that they were not thoroughly recorded). Despite justifiable scepticism, feasibility analyses demonstrated that meaningful explorations of the aggregate dataset, composed of 24 imaging sites for a grand total of 1093 subjects, could be performed (Biswal et al., 2010). Although no explicit correction for multi-site variability was used, they only use global signal correction (GSC) to normalize subjects which may introduce anti-correlation in the data (Fox et al., 2009; Murphy et al., 2009; Saad et al., 2012; Carbonell et al., 2014; Power et al., 2014). After accounting for site-related differences, the analysis showed brain-behaviour relationships with phenotypic variables such as age, gender, and diagnostic label, and confirmed a variety of prior hypotheses (Biswal et al., 2010; Fair et al., 2012; Tomasi and Volkow, 2010; Zuo et al., 2012). While encouraging, many uncontrolled and unknown factors in the 1000 FCP remain a source of concern, as they spread beyond simple site effects and can limit the datasets utility as highlighted by Yan et al. (2013a). An other compelling proof of multi-site bias is the study reported by Nielsen et al. (2013) where they did an analysis on a single site dataset and a multi-site dataset of subject with autism and concluded that

the multi-site autism study classification accuracy significantly outperformed chance but was much lower for multi-site prediction than for previous single site results (Nielsen et al., 2013). We therefore need to keep in mind that the site effect must be taken in account in the analysis or we may reduce our detection power.

Specific objectives.

- Propose methods to account for multisite variance in a general linear model analysis
- Amount of variance intra-site and inter-site
- How group balancing in multi-centric topology impact sensitivity
- How sample size in multi-centric topology impact sensitivity
- Interaction of

2. Method

2.1. Data samples

Participants. The paper studies 313 elderly adults with and without cognitive impairment of the Alzheimer type collected across 5 studies: ADNI2 study and 4 other studies based in Montreal, Canada (from the ADMTL dataset), for a grand total of 126 CNE participants (51 males, age range = 57-94 yrs), 133 patients with MCI (70 males, age range = 55-89 yrs), and 54 patients with DAT (22 males, age range = 55-88 yrs) (see table ??). We have also included 355 cognitively normal young adults (CNY) from the 1000 functional connectome project¹ (150 males, age range = 18-46 yrs) as a reference dataset.

Acquisition.

2.2. Preprocessing

The datasets were analysed using the NeuroImaging Analysis Kit (NIAK²) version 0.12.14, under CentOS version 6.3 with Octave³ version 3.8.1 and the Minc toolkit⁴ version 0.3.18. Analyses were executed in parallel on the "Mammouth" supercomputer⁵, using the pipeline system for Octave and Matlab (Belléc et al., 2010a), version 1.0.2. Brain map visualizations were created using MRICron software Rorden et al. (2007). Each fMRI dataset was corrected

¹http://fcon_1000.projects.nitrc.org/

²<http://www.nitrc.org/projects/niak/>

³<http://gnu.octave.org>

⁴<http://www.bic.mni.mcgill.ca/ServicesSoftware/ServicesSoftwareMincToolKit>

⁵<http://www.calculquebec.ca/index.php/en/resources/compute-servers/mammouth-parallel-ii>

of inter-slice difference in acquisition time and the parameters of a rigid-body motion was estimated for each time frame. Rigid-body motion was estimated within as well as between runs, using the median volume of the first run as a target. The median volume of one selected fMRI run for each subject was coregistered with a T1 individual scan using Minctracc (Collins et al., 1998), which was itself non-linearly transformed to the Montreal Neurological Institute (MNI) template (Fonov et al., 2011) using the CIVET pipeline (Zijdenbos et al., 2002). The MNI symmetric template was generated from the ICBM152 sample of 152 young adults, after 40 iterations of non-linear coregistration. The rigid-body transform, fMRI-to-T1 transform and T1-to-stereotaxic transform were all combined, and the functional volumes were resampled in the MNI space at a 3 mm isotropic resolution. The a censoring method described in (Power et al., 2012) called "scrubbing" was used to remove the volumes with excessive motion using a cut-off value of $FD \geq 0.5$. A minimum number of 50 unscrubbed volumes per run, corresponding to ~ 125 s of acquisition for a TR of 2.5 seconds, was then required for further analysis. The following nuisance parameters were regressed out from the time series at each voxel: slow time drifts (basis of discrete cosines with a 0.01 Hz high-pass cut-off), average signals in conservative masks of the white matter and the lateral ventricles as well as the first principal components (95% energy) of the six rigid-body motion parameters and their squares (Lund et al., 2006),(Giove et al., 2009). The fMRI volumes were finally spatially smoothed with a 6 mm isotropic Gaussian blurring kernel.

2.3. Feature selection

Regions are routinely defined using an anatomical parcellation (He et al., 2009), such as the AAL template (Tzourio-Mazoyer et al., 2002). Anatomical parcels may however not well match the organization of resting-state networks. The BASC method was used to generate data-driven functional decomposition into resting-state networks based on the coherence of BOLD activity at the individual or group level (Bellec, 2006; Bellec et al., 2010b; Bellec, 2013). When a low number of networks (or scale) is used, the brain got decomposed into distributed large-scale networks, such as the DMN. At high scales (large number of networks), the BASC identified subnetworks and functional regions (Kelly et al., 2012). We generated a BASC parcellation in 100 clusters on the Cambridge sample, including ~ 200 young adults from the 1000 functional connectome database (Biswal et al., 2010) and used it to generate the rs-fMRI outcome measures.

The default-mode network. Since the seminal work of Greicius et al. (2004), many rs-fMRI studies in AD focused on the default-mode network (DMN), a group of regions consistently more active at rest than during a broad range of different tasks (Gusnard and Raichle, 2001). The DMN was notably reported to largely overlap with the regions that show high amyloid-beta deposition in patients with DAT (Buckner et al., 2009). It includes the posterior cingulate cortex (PCC) / Precuneus (PCUN) area, the inferior parietal lobule (IPL), the anterior cingulate cortex / medial prefrontal cortex (MPFC) (Greicius et al.,

2003). Other structures such as the medial temporal cortex or the superior frontal gyrus are also generally regarded as part of different subnetworks of the DMN (Margulies et al., 2009; Andrews-Hanna et al., 2010).

Literature review: Alzheimer's disease and resting-state fMRI. We performed a literature review to select candidate connections that have been shown to be prominently impacted in Alzheimer's disease. There is no single authoritative reference on the effect of a DAT on rs-fMRI connectivity, and the field has been dominated thus far by studies with small samples ($n \sim 20$) and limited statistical power, see Sheline and Raichle (2013) for a recent review. Because the DMN has been most extensively studied, we decided to focus on this network and to run a meta-analysis on six papers that (1) used some analogue of seed-based connectivity maps in resting-state fMRI using one or multiple seeds in the DMN (2) investigated abnormalities in resting-state functional connectivity in patients suffering of a dementia of the Alzheimer's type and (3) provided tables of coordinates in stereotaxic space for the results.

review: Alzheimer's disease and resting-state fMRI.

- Zhang et al. (2009) used functional connectivity maps with a seed in the posterior cingulate cortex (PCC) to explore the differences between a group of elderly cognitively normal subjects (CNE, $n=16$) and patients with a mild dementia of the Alzheimer's type (DAT, $n=18$).
- Zhang et al. (2010) generalized the Zhang et al. (2009) study with CNE ($n=16$) and a larger group of patients with DAT ($n=46$). Patients were separated in three groups (mild, moderate, severe DAT), and each group of patients was contrasted against the CNE.
- Wang et al. (2006) used functional connectivity maps with a seed in the hippocampi to explore the differences between a group of CNE ($n=13$) and patients with a mild DAT ($n=13$). All results included in the meta-analysis are from Table 2, seeded in the right hippocampus. Seeds were manually delineated on an individual basis.
- Wang et al. (2007) used functional connectivity maps with a seed in the posterior cingulate cortex (PCC) as well as full brain point-to-point correlations (based on an AAL parcellation) to explore the differences between a group of elderly cognitively normal subjects (CNE, $n=14$) and patients with a very mild to mild dementia of the Alzheimer's type (DAT, $n=14$). Only the results based on the PCC seed were included in the meta-analysis.
- Goveas et al. (2011) used functional connectivity maps with a seed in the hippocampi to explore the differences between a group of elderly cognitively normal subjects (CNE, $n=18$) and patients with a mild dementia of the Alzheimer's type (DAT, $n=14$) before and after donepezil treatment. Seeds were manually delineated on an individual basis, before and after treatment.

- Damoiseaux et al. (2012) used dual-regression independent component analysis to explore longitudinal differences between a group of CNE (n=18) and patients with DAT (n=21). All results included in the meta-analysis are from Table 3 (differences at baseline) and Table 4 (interaction with time). The authors used three components representing the Anterior DMN, Ventral DMN and Posterior DMN.

To assess the degree of consistency of the findings across studies, we counted the number of coordinates located in each one of the BASC regions. The resulting map is presented in Figure 2. As can be seen, there is a lot of variability across studies, with only a limited number of regions reaching a score above 3 (i.e. reported in at least 3 of the contrasts in the six studies). Note that we did not select connections with the hippocampus, although this region was frequently reported. The rationale was that the drug effects on this area are expected to be minimal in patients with a moderate DAT, because the very severe atrophy of the structure cannot be recovered. In the regions showing the most consistency (score of 3 or more), there were many regions located in the DMN, such as the PCC, the PCUN, the IPL (a bilateral node), the right superior frontal gyrus (SFG), as well as two dorsal MPFC cortex (dMPFC and dMPFC2) and an anterior MPFC parcel (aMPFC). Three parcels were found in the visual network: the lingual gyrus (LING), the fusiform gyrus (FUS) and a dorso-medial occipital (DMO) parcel. Two parcels were found in the dorsal attentional network: the intra-parietal sulcus (IPS) and the motor part of the precuneus (PCUNm, see Margulies et al. (2009)). One parcel was found in the premotor cortex (PMC), associated with the sensorimotor network, one parcel in the left dorsolateral prefrontal cortex (rDLPFC), associated with the fronto-parietal task-control network, as well as a parcel in the dMPFC (dMPFC3) associated with the cingulo-opercular cortex. Finally, a parcel included the temporal poles (TPo) bilaterally. Note that the nomenclature for distributed networks was based on (Power et al., 2011).

The TRT reliability study was based on the publicly available NYU-TRT database. The database included 25 young healthy adults, and each subject had three rs-fMRI run: two in a single session (separated by 45 mns) and another run 5 – 16 months latter. Several outcome measures were generated in key regions impacted by AD. Using the three runs, one intra-class correlation (ICC) was generated intra-session, and two ICCs were generated inter-session for each outcome measures. The outcome measures were ranked based on average of intra- and inter-session ICCs.

2.4. Simulations

Parcellation. Functional brain parcellation into 300 regions was obtained from reference dataset of healthy adults from the 1000 functional connectome project (Cambridge cohort, parcelation available here ??). To do so the spatial dimension of the independent individual fMRI dataset was reduced to 957 regions using a region-growing algorithm Bellec (2006) and final network decomposition

was obtained using BASC Bellec et al. (2010b) a bootstrap method to identify stable networks at various scales.

2.5. Functional network

Regions are routinely defined using an anatomical parcellation (He et al., 2009), such as the AAL template (Tzourio-Mazoyer et al., 2002). Anatomical parcels may however not well match the organization of resting-state networks. We use a framework to generate data-driven functional decomposition into resting-state networks based on the coherence of BOLD activity at the individual or group level (Bellec, 2006),(Bellec et al., 2010b). When a low number of networks (or scale) is used, this technique, called bootstrap analysis of stable clusters (BASC), generates decompositions of the brain into distributed large-scale networks, such as the DMN. At high scales, it identifies subnetworks and functional regions (Kelly et al., 2012). We generated a BASC parcellation with a 100 clusters on the Cambridge sample, including ~ 200 young adults from the 1000 functional connectome database (Biswal et al., 2010) and used it to generate the rs-fMRI outcome measures.

Functional maps. For each run, the correlation matrix was generated base on the time series averaged on the parcellation of an independent dataset mention previously (Cambridge 100 parcels). For each subject, the connectomes were averaged across all runs. The following region posterior cingulate cortex (PCC), a central node of the default mode network, was used to generate seed based connectivity maps. Finally, the average voxelwise functional connectivity maps was generated, i.e. Pearson's correlation corrected by the Fisher transform and averaged across all runs for each subject.

2.6. Statistical analysis

Dataset. In order to simulate various scenarios within the context of a multi-site setting, a cohort of subjects acquired at a single-site was selected to act as our reference dataset and for the multi-site configuration a cohort from a collection of 7 small sites, roughly totalling the same sample size as the reference dataset, was used. The cohort used for the study contains 385 participants from the 1000 Functional Connectomes Project (Biswal et al., 2010) (150 males, age range = 18-46 yrs) composed of 1 large site (Cambridge $n=\sim 200$) and 7 small sites ($n=\sim 20$ /site for a total ~ 200). The fMRI datasets were preprocessed with the Neuro-Imaging Analysis Kit (NIAK) as described earlier in Section 2.2.

Functional connectome. Using a brain partition of R networks obtain from BASC procedure described in Bellec et al. (2010b), and taking each pair of distinct networks i and j , the between-network connectivity $y_{i,j}$ is measured by the Fisher transform of the Pearson's correlation between the average time series of the network. The within-network connectivity $y_{i,i}$ is the Fisher transform of the average correlation between time series of every pair of distinct voxels inside network i . The connectome $\mathbf{Y} = (y_{i,j})_{i,j=1}^R$ is thus a $R \times R$ matrix. Each column j (or row, as the matrix is symmetric) codes for the connectivity between

network j and all other brain networks (full brain functional connectivity map). For a scale with R parcels, there are exactly $L = R(R + 1)/2$ distinct elements in an individual connectome \mathbf{Y} .

Point-to-point connections. Based on the literature review previously described the connectivity between 10 reproducible pair of regions were selected based on the criteria that they were impacted by the disease (specifically the pDAT-CNE contrast) in a literature review.

Estimation of the detection sensitivity. The following confounding variables were modelled in the GLM analysis: frame displacement (FD), age and gender. Significance of the results is obtain with a Student t -test and the sensitivity of the test is evaluated by sub-sampling 70% of the dataset ($B = 10^4$ random samples). For each sample b , we have a p -value p_b^* and the detection sensitivity is estimated by the probability of p_b^* being inferior to 0.05.

$$\frac{1}{B} \sum_{b=1}^B (p_b^* \leq 0.05). \quad (1)$$

Effect size (cohen's d). For each site and each sample, half of the subjects were randomly assigned to a "treatment" group and a Monte-Carlo simulation was used to estimate the detection power in the single-site and in multi-site setting.

The normalized Cohen's d was used to estimate the effect size and it is defined as the difference between two means \bar{x}_1, \bar{x}_2 divided by a standard deviation from the data s .

For each site an effect is added to the connectivity of 50% of the subjects, selected randomly ("pathological" group):

$$y_{i,j} = y_{i,j} + \mu. \quad (2)$$

The parameter μ is chosen to obtain a particular effect size (measured by the Cohen d)

$$d = \frac{\mu}{s_{i,j}}, \quad (3)$$

where $s_{i,j}$ is the standard deviation between region i and j for the reference population (mono-site, Cambridge). The significance of the difference between the control and 'treatment' group was assessed by a t -test in a linear model, including a covariate to model the motion. The study was repeated for various effect sizes (0 to 0.8 with a step of 0.01) with a p -value threshold of 0.05 on the t -test.

multi-site correction approaches. For the multi-site three flavours were computed: multi-site no correction, multi-site with dummy variables and multi-site with METAL correction. Depending on the multi-site configuration and distribution of the subject we proposed two corrective approaches that can be applied as shown in the simulations of Figure 9. The first one is the introduction of dummy variables (binary vectors $1 \times N$) who code for each site in the GLM model ??.

The variables are corrected to have a zero mean across subjects, and an intercept (i.e. a column filled with 1) is added to \mathbf{X} . The GLM relies on the following stochastic model:

$$\mathbf{Y} = \mathbf{X}\beta + \mathbf{V}\gamma + \mathbf{E}, \quad (4)$$

- \mathbf{Y} : $N \times 1$, connectivity value for the pair (i, j) ,
- \mathbf{X} : $N \times K$, explainable variables,
- β : $1 \times K$, regression values for each explainable variable,
- \mathbf{V} : $N \times S$, each column code for a site (0/1),
- γ : $1 \times S$, site average connectivity,
- \mathbf{E} : $N \times 1$, residual values from the regression,

with N the number of subjects, K the number of explainable variables, S the number of sites.

where β is an unknown $C \times L$ matrix of linear regression coefficients and \mathbf{E} is a $N \times L$ random (noise) multivariate Gaussian variable. To apply the correction $v - 1$ dummy-variables are added to the model ?? with v being the total number of sites used in the study.

The second approach is to compute the GLM independently on each site and then combine the statistical results from each site in a global score. This model averaging technique called METAL from Willer et al. (2010) model site specific bias by running a GLM analysis on each site resulting in v beta vectors that are weighted proportionally to the standard error of each site and finally averaged as shown in equation 10. This is the most flexible way to account for multi-site effect while keeping the analysis simple and robust to unbalanced sites.

$$\beta_v, \text{ effect size estimate for site } v. \quad (5)$$

$$\sigma_v, \text{ standard error for site } v. \quad (6)$$

$$w_v = \frac{1}{\sigma_v^2}, \text{ weight estimate for site } v. \quad (7)$$

$$\beta = \frac{\sum_v \beta_v w_v}{\sum_v w_v}, \text{ global } \beta. \quad (8)$$

$$\sigma = \sqrt{\frac{1}{\sum_v w_v}}, \text{ global standard error.} \quad (9)$$

$$Z = \frac{\beta}{\sigma}, \text{ global Z score.} \quad (10)$$

$$p = 2(1 - \phi(|Z|)), \text{ p-value.} \quad (11)$$

Frame-wise displacement (FD). Index measure of head motion from one frame to the other. It is calculated as the sum of the absolute values of the differentiated realignment estimates at every time point (Power et al., 2012) this measure give us an approximation of the motion frame by frame in millimeter. We are using this measure as an index of motion estimation.

$$FD_i = |\Delta d_x(t)| + |\Delta d_y(t)| + |\Delta d_z(t)| + |\Delta r_x(t)| + |\Delta r_y(t)| + |\Delta r_z(t)|, \quad (12)$$

$$r_x(t) = 50 \left(\frac{2\pi\alpha_x(t)}{360} \right), \quad (13)$$

with

- $(d_x(t), d_y(t), d_z(t))$ translation parameters (mm),
- $(\alpha_x(t), \alpha_y(t), \alpha_z(t))$ rotation parameters (degrees),
- Δ difference between time t et $t - 1$.

3. Results

The Figure 1 presents the results of the ICC analysis for the point-to-point correlations, only the connections with an average ICC above 0.5 are represented. The results were consistent with (Shehzad et al., 2009), with a mean ICC over all connections of ~0.3 and 23 connections scoring a moderate-to-good level of ICC (> 0.5).

Average connectivity maps associated with the DMN nodes as well as the nodes outside the DMN that passed the TRT selection are presented in Figures 3 and 4. The involvement of the sensorimotor, visual and attentional networks mainly came from contrasts reporting a decrease of negative correlations in patients, that was interpreted as a compensation mechanism by some authors. These connections are potentially very valuable to monitor the effect of a drug. Considering that we pooled studies of the DMN, we decided to select as candidates all connections of parcels within the DMN, as well as connections between a parcel inside the DMN and a parcel outside the DMN. The final selection of target measures was based on test-retest reliability. All the parcels and associated labels and networks are listed in Table 1.

For point-to-point correlations within the DMN, we selected the connections with highest ICC for each node (all average ICC > 0.5):

- PCC x PCUN
- dMPFC x dMPFC2
- IPL x SFGr
- aMPFC x PCUN

For each point-to-point correlation between the DMN and another network, we selected the connections with highest ICC and $\text{ICC} \geq 0.5$:

- FUS x SFG_r
- PCC x PCUNm
- IPL x dMPFC3

The first assessment perform on the dataset was to verify the distribution of the variance in functional connectivity among each site and across sites in order to see if they are of the same order of magnitude or not. This analysis of Figure 5 shows the distribution of the standard deviation of connectivity across subjects (the distribution is over the full brain connectome, with several 1000s connections) at the 8 sites against the inter-sites standard deviation of connectomes (average at each site). as we can see the inter-site (between site) variability is smaller than the intra-site (between subjects) variability.

In order to verify how spatial structure vary across sites the average standard deviation and the average connectivity map of the DMN was extracted for each site and displayed in Figure 7. In order to ease the reading we selected only 4 representative sites, although we reached the same conclusion on all the sites. As we can see in the intersection between two sites the difference in standard deviation between-sites was illustrated (red set of brain cuts). First the mean DMN at each site is consistent with the expected spatial ditribution reported in other studies. As we can see the amplitude of inter-site bias is about 3-fold smaller than the within-site standard deviation (red ~ 0.06 vs. orange ~ 0.18). The most salient changes between-sites are located in the mesio-frontal region associated with the anterior part of the DMN. This last finding may be associated with motion artefact as previously reported in Dansereau et al. (2014).

We also showed using Monte-Carlo simulations that the power of detecting an effect is marginally affected by the site acquisition configuration (single site or multi-site, see Figure3.2 for an illustration of a power analysis on three different seeds) where the sites are balanced in term of the amount of subject with and without the effect.

4. Conclusion

We confirmed that multi-site acquisition introduce some variability in the dataset although a single-site study with 200 subjects had only a marginally superior statistical power than an analysis pooling 7 sites for an equivalent number of subjects, see Figure 8. In both cases, a high sensitivity (> 0.95) could be achieved for the effect size observed by Goveas et al. (2011) which reported an effect equivalent to 1. We can therefore conclude that it is feasible to acquire rs-fMRI data in across multiple sites and correct for this topology.

5. Acknowledgments

Parts of this work were presented at the 2013 annual meetings of the organization for human brain mapping (Dansereau et al., 2013), as well as the Alzheimer’s Association International Conference (AAIC) (2014) (Copenhagen) (Dansereau et al., 2014). The authors are grateful to the members of the 1000 functional connectome consortium for publicly releasing there dataset. The computational resources used to perform the data analysis were provided by ComputeCanada⁶ and CLUMEQ⁷, which is funded in part by NSERC (MRS), FQRNT, and McGill University. This project was funded by NSERC grant number RN000028, a salary award from “Fonds de recherche du Québec – Santé” to PB as well as a salary award by the Canadian Institute of Health Research to CD.

References

- Andrews-Hanna, J. R., Reidler, J. S., Sepulcre, J., Poulin, R., Buckner, R. L., Feb. 2010. Functional-anatomic fractionation of the brain’s default network. *Neuron* 65 (4), 550–562.
URL <http://dx.doi.org/10.1016/j.neuron.2010.02.005>
- Bellec, P., Feb. 2006. Longitudinal study of large-scale networks in the human brain using fMRI : Methods and application to motor skill learning. Ph.D. thesis, Université Paris XI, Orsay, Paris.
URL http://exocet.imed.jussieu.fr/~pbellec/data/these_bellec.pdf
- Bellec, P., 2013. Mining the hierarchy of resting-state brain networks: selection of representative clusters in a multiscale structure. In: Pattern Recognition in Neuroimaging (PRNI), 2013 International Workshop on. IEEE, pp. 54–57.
- Bellec, P., Carbonell, F., Perlberg, V., Evans, A. C., 2010a. A neuroimaging analysis kit for Octave and Matlab.
URL <http://code.google.com/p/niak/>
- Bellec, P., Rosa-Neto, P., Lyttelton, O. C., Benali, H., Evans, A. C., Jul. 2010b. Multi-level bootstrap analysis of stable clusters in resting-state fMRI. *NeuroImage* 51 (3), 1126–1139.
URL <http://dx.doi.org/10.1016/j.neuroimage.2010.02.082>
- Biswal, B. B., Mennes, M., Zuo, X.-N. N., Gohel, S., Kelly, C., Smith, S. M., Beckmann, C. F., Adelstein, J. S., Buckner, R. L., Colcombe, S., Dogonowski, A.-M. M., Ernst, M., Fair, D., Hampson, M., Hoptman, M. J., Hyde, J. S., Kiviniemi, V. J., Kötter, R., Li, S.-J. J., Lin, C.-P. P., Lowe, M. J., Mackay,

⁶<https://compute-canada.org/>

⁷<http://www.clumeq.mcgill.ca/>

C., Madden, D. J., Madsen, K. H., Margulies, D. S., Mayberg, H. S., McMahon, K., Monk, C. S., Mostofsky, S. H., Nagel, B. J., Pekar, J. J., Peltier, S. J., Petersen, S. E., Riedl, V., Rombouts, S. A., Rypma, B., Schlaggar, B. L., Schmidt, S., Seidler, R. D., Siegle, G. J., Sorg, C., Teng, G.-J. J., Veijola, J., Villringer, A., Walter, M., Wang, L., Weng, X.-C. C., Whitfield-Gabrieli, S., Williamson, P., Windischberger, C., Zang, Y.-F. F., Zhang, H.-Y. Y., Castellanos, F. X., Milham, M. P., Mar. 2010. Toward discovery science of human brain function. *Proceedings of the National Academy of Sciences of the United States of America* 107 (10), 4734–4739.

URL <http://dx.doi.org/10.1073/pnas.0911855107>

Buckner, R. L., Sepulcre, J., Talukdar, T., Krienen, F. M., Liu, H., Hedden, T., Andrews-Hanna, J. R., Sperling, R. A., Johnson, K. A., Feb. 2009. Cortical hubs revealed by intrinsic functional connectivity: mapping, assessment of stability, and relation to Alzheimer's disease. *The Journal of neuroscience : the official journal of the Society for Neuroscience* 29 (6), 1860–1873.

URL <http://dx.doi.org/10.1523/JNEUROSCI.5062-08.2009>

Carbonell, F., Bellec, P., Shmuel, A., Feb 2014. Quantification of the impact of a confounding variable on functional connectivity confirms anti-correlated networks in the resting-state. *Neuroimage* 86, 343–353.

URL <http://dx.doi.org/10.1016/j.neuroimage.2013.10.013>

Cho, Z. H., Chung, S. C., Lim, D. W., Wong, E. K., Feb 1998. Effects of the acoustic noise of the gradient systems on fmri: a study on auditory, motor, and visual cortices. *Magn Reson Med* 39 (2), 331–335.

Collins, D. L., Zijdenbos, A. P., Kollokian, V., Sled, J. G., Kabani, N. J., Holmes, C. J., Evans, A. C., Jun. 1998. Design and construction of a realistic digital brain phantom. *IEEE Trans Med Imaging* 17 (3), 463–468.

URL <http://view.ncbi.nlm.nih.gov/pubmed/9735909>

Cullen, K. R., Gee, D. G., Klimes-Dougan, B., Gabbay, V., Hulvershorn, L., Mueller, B. A., Camchong, J., Bell, C. J., Houry, A., Kumra, S., Lim, K. O., Castellanos, F. X., Milham, M. P., Sep 2009. A preliminary study of functional connectivity in comorbid adolescent depression. *Neurosci Lett* 460 (3), 227–231.

URL <http://dx.doi.org/10.1016/j.neulet.2009.05.022>

Damoiseaux, J. S., Prater, K. E., Miller, B. L., Greicius, M. D., Apr. 2012. Functional connectivity tracks clinical deterioration in Alzheimer's disease. *Neurobiology of Aging* 33 (4), 828.e19–828.e30.

URL <http://dx.doi.org/10.1016/j.neurobiolaging.2011.06.024>

Dansereau, C., Orban, P., Bellec, P., 2014. Impact of motion on resting-state fmri connectivity in healthy aging and alzheimer's disease, and possible remedies. Vol. 10. pp. P49 –, alzheimer's Association International Conference 2014 Alzheimer's Association International Conference 2014.

URL <http://www.sciencedirect.com/science/article/pii/S1552526014007389>

Dansereau, C., Risterucci, C., Pich, E. M., Arnold, D., Bellec, P., 2013. A power analysis for multisite studies in resting-state functional connectivity, with an application to clinical trials in alzheimer's disease. Vol. 9. pp. P248 – P249, alzheimer's Association International Conference 2013 Alzheimer's Association International Conference 2013.

URL <http://www.sciencedirect.com/science/article/pii/S1552526013011461>

Desmond, J., Glover, G., Aug. 2002. Estimating sample size in functional mri (fmri) neuroimaging studies: Statistical power analyses. Journal of Neuroscience Methods 118 (2), 115–128.

URL [http://dx.doi.org/10.1016/s0165-0270\(02\)00121-8](http://dx.doi.org/10.1016/s0165-0270(02)00121-8)

Edward, V., Windischberger, C., Cunningham, R., Erdler, M., Lanzenberger, R., Mayer, D., Endl, W., Beisteiner, R., Nov 2000. Quantification of fmri artifact reduction by a novel plaster cast head holder. Hum Brain Mapp 11 (3), 207–213.

Elliott, M. R., Bowtell, R. W., Morris, P. G., Jun 1999. The effect of scanner sound in visual, motor, and auditory functional mri. Magn Reson Med 41 (6), 1230–1235.

Fair, D. A., Nigg, J. T., Iyer, S., Bathula, D., Mills, K. L., Dosenbach, N. U. F., Schlaggar, B. L., Mennes, M., Gutman, D., Bangaru, S., Buitelaar, J. K., Dickstein, D. P., Martino, A. D., Kennedy, D. N., Kelly, C., Luna, B., Schweitzer, J. B., Velanova, K., Wang, Y.-F., Mostofsky, S., Castellanos, F. X., Milham, M. P., 2012. Distinct neural signatures detected for adhd subtypes after controlling for micro-movements in resting state functional connectivity mri data. Front Syst Neurosci 6, 80.

URL <http://dx.doi.org/10.3389/fnsys.2012.00080>

Fang, F., Murray, S. O., He, S., Jun 2007. Duration-dependent fmri adaptation and distributed viewer-centered face representation in human visual cortex. Cereb Cortex 17 (6), 1402–1411.

URL <http://dx.doi.org/10.1093/cercor/bhl053>

Feinberg, D. A., Moeller, S., Smith, S. M., Auerbach, E., Ramanna, S., Gunther, M., Glasser, M. F., Miller, K. L., Ugurbil, K., Yacoub, E., 2010. Multiplexed echo planar imaging for sub-second whole brain fmri and fast diffusion imaging. PLoS One 5 (12), e15710.

URL <http://dx.doi.org/10.1371/journal.pone.0015710>

Fonov, V., Evans, A. C., Botteron, K., Almlí, C. R., McKinstry, R. C., Collins, D. L., Brain Development Cooperative Group, Jan. 2011. Unbiased average age-appropriate atlases for pediatric studies. NeuroImage 54 (1), 313–327.

URL <http://dx.doi.org/10.1016/j.neuroimage.2010.07.033>

- Fox, M. D., Zhang, D., Snyder, A. Z., Raichle, M. E., Jun 2009. The global signal and observed anticorrelated resting state brain networks. *J Neurophysiol* 101 (6), 3270–3283.
URL <http://dx.doi.org/10.1152/jn.90777.2008>
- Friedman, L., Glover, G., Jun. 2006. Report on a multicenter fmri quality assurance protocol. *Journal of magnetic resonance imaging : JMRI* 23 (6), 827–839.
URL <http://dx.doi.org/10.1002/jmri.20583>
- Friedman, L., Glover, G., Consortium, T. F., Nov. 2006. Reducing interscanner variability of activation in a multicenter fmri study: Controlling for signal-to-fluctuation-noise-ratio (sfnr) differences. *NeuroImage* 33 (2), 471–481.
URL <http://dx.doi.org/10.1016/j.neuroimage.2006.07.012>
- Giove, F., Gili, T., Iacobella, V., Macaluso, E., Maraviglia, B., Oct. 2009. Images-based suppression of unwanted global signals in resting-state functional connectivity studies. *Magnetic resonance imaging* 27 (8), 1058–1064.
URL <http://dx.doi.org/10.1016/j.mri.2009.06.004>
- Goveas, J. S., Xie, C., Ward, B. D., Wu, Z., Li, W., Franczak, M., Jones, J. L., Antuono, P. G., Li, S.-J. J., Oct. 2011. Recovery of hippocampal network connectivity correlates with cognitive improvement in mild Alzheimer's disease patients treated with donepezil assessed by resting-state fMRI. *Journal of magnetic resonance imaging : JMRI* 34 (4), 764–773.
URL <http://dx.doi.org/10.1002/jmri.22662>
- Greicius, M. D., Krasnow, B., Reiss, A. L., Menon, V., Jan. 2003. Functional connectivity in the resting brain: A network analysis of the default mode hypothesis. *Proc. Natl. Acad. Sci.* 100 (1), 253–258.
URL <http://dx.doi.org/10.1073/pnas.0135058100>
- Greicius, M. D., Srivastava, G., Reiss, A. L., Menon, V., Mar. 2004. Default-mode network activity distinguishes Alzheimer's disease from healthy aging: Evidence from functional MRI. *Proceedings of the National Academy of Sciences of the United States of America* 101 (13), 4637–4642.
URL <http://dx.doi.org/10.1073/pnas.0308627101>
- Gusnard, D. A., Raichle, M. E., Oct. 2001. Searching for a baseline: Functional imaging and the resting human brain. *Nature Reviews Neuroscience* 2 (10), 685–694.
URL <http://dx.doi.org/10.1038/35094500>
- Hartstra, E., Khn, S., Verguts, T., Brass, M., Nov 2011. The implementation of verbal instructions: an fmri study. *Hum Brain Mapp* 32 (11), 1811–1824.
URL <http://dx.doi.org/10.1002/hbm.21152>
- He, Y., Chen, Z., Gong, G., Evans, A., Aug. 2009. Neuronal networks in Alzheimer's disease. *The Neuroscientist : a review journal bringing neurobiology, neurology and psychiatry* 15 (4), 333–350.
URL <http://dx.doi.org/10.1177/1073858409334423>

- Kelly, C., Toro, R., Di Martino, A., Cox, C. L., Bellec, P., Castellanos, F. X., Milham, M. P., Jul. 2012. A convergent functional architecture of the insula emerges across imaging modalities. *NeuroImage* 61 (4), 1129–1142.
URL <http://dx.doi.org/10.1016/j.neuroimage.2012.03.021>
- Klarhofer, M., Barth, M., Moser, E., May 2002. Comparison of multi-echo spiral and echo planar imaging in functional mri. *Magn Reson Imaging* 20 (4), 359–364.
- Lin, F.-H., Huang, T.-Y., Chen, N.-K., Wang, F.-N., Stufflebeam, S. M., Belliveau, J. W., Wald, L. L., Kwong, K. K., Aug 2005. Functional mri using regularized parallel imaging acquisition. *Magn Reson Med* 54 (2), 343–353.
URL <http://dx.doi.org/10.1002/mrm.20555>
- Lund, T. E., Madsen, K. H., Sidaros, K., Luo, W.-L., Nichols, T. E., Jan. 2006. Non-white noise in fMRI: does modelling have an impact? *NeuroImage* 29 (1), 54–66.
URL <http://dx.doi.org/10.1016/j.neuroimage.2005.07.005>
- Margulies, D. S., Vincent, J. L., Kelly, C., Lohmann, G., Uddin, L. Q., Biswal, B. B., Villringer, A., Castellanos, F. X., Milham, M. P., Petrides, M., Nov. 2009. Precuneus shares intrinsic functional architecture in humans and monkeys. *Proceedings of the National Academy of Sciences of the United States of America*.
URL <http://dx.doi.org/10.1073/pnas.0905314106>
- Menon, V., Lim, K., Anderson, J., Johnson, J., Pfefferbaum, A., 1997. Design and efficacy of a head-coil bite bar for reducing movement-related artifacts during functional mri scanning. *Behavior Research Methods, Instruments, & Computers* 29 (4), 589–594.
URL <http://dx.doi.org/10.3758/BF03210613>
- Mueller, S. G., Weiner, M. W., Thal, L. J., Petersen, R. C., Jack, C., Jagust, W., Trojanowski, J. Q., Toga, A. W., Beckett, L., Nov 2005. The alzheimer's disease neuroimaging initiative. *Neuroimaging Clin N Am* 15 (4), 869–77, xi-xii.
URL <http://dx.doi.org/10.1016/j.nic.2005.09.008>
- Murphy, K., Birn, R. M., Handwerker, D. A., Jones, T. B., Bandettini, P. A., Feb. 2009. The impact of global signal regression on resting state correlations: are anti-correlated networks introduced? *NeuroImage* 44 (3), 893–905.
URL <http://dx.doi.org/10.1016/j.neuroimage.2008.09.036>
- Nielsen, J., Zielinski, B., Fletcher, T., Alexander, A., Lange, N., Bigler, E., Lainhart, J., Anderson, J., 2013. Multisite functional connectivity mri classification of autism: Abide results. *Frontiers in human neuroscience* 7, –.
URL <http://view.ncbi.nlm.nih.gov/pubmed/24093016>

- Power, J. D., Barnes, K. A., Snyder, A. Z., Schlaggar, B. L., Petersen, S. E., Feb. 2012. Spurious but systematic correlations in functional connectivity MRI networks arise from subject motion. *NeuroImage* 59 (3), 2142–2154.
 URL <http://dx.doi.org/10.1016/j.neuroimage.2011.10.018>
- Power, J. D., Cohen, A. L., Nelson, S. M., Wig, G. S., Barnes, K. A., Church, J. A., Vogel, A. C., Laumann, T. O., Miezin, F. M., Schlaggar, B. L., Petersen, S. E., Nov. 2011. Functional Network Organization of the Human Brain. *Neuron* 72 (4), 665–678.
 URL <http://dx.doi.org/10.1016/j.neuron.2011.09.006>
- Power, J. D., Mitra, A., Laumann, T. O., Snyder, A. Z., Schlaggar, B. L., Petersen, S. E., Jan. 2014. Methods to detect, characterize, and remove motion artifact in resting state fMRI. *NeuroImage* 84, 320–341.
 URL <http://dx.doi.org/10.1016/j.neuroimage.2013.08.048>
- Rorden, C., Karnath, H.-O., Bonilha, L., Jul 2007. Improving lesion-symptom mapping. *J Cogn Neurosci* 19 (7), 1081–1088.
 URL <http://dx.doi.org/10.1162/jocn.2007.19.7.1081>
- Saad, Z. S., Gotts, S. J., Murphy, K., Chen, G., Jo, H. J. J., Martin, A., Cox, R. W., 2012. Trouble at rest: how correlation patterns and group differences become distorted after global signal regression. *Brain connectivity* 2 (1), 25–32.
 URL <http://dx.doi.org/10.1089/brain.2012.0080>
- Shehzad, Z., Kelly, C. M., Reiss, P. T., Gee, D. G., Gotimer, K., Uddin, L. Q., Lee, S. H. H., Margulies, D. S., Roy, A. K. K., Biswal, B. B., Petkova, E., Castellanos, F. X., Milham, M. P., Oct. 2009. The resting brain: unconstrained yet reliable. *Cerebral cortex* (New York, N.Y. : 1991) 19 (10), 2209–2229.
 URL <http://dx.doi.org/10.1093/cercor/bhn256>
- Sheline, Y., Raichle, M., Sep. 2013. Resting state functional connectivity in preclinical alzheimers disease. *Biological Psychiatry* 74 (5), 340–347.
 URL <http://dx.doi.org/10.1016/j.biopsych.2012.11.028>
- Tomasi, D., Volkow, N. D., May 2010. Functional connectivity density mapping. *Proceedings of the National Academy of Sciences* 107 (21), 9885–9890.
 URL <http://dx.doi.org/10.1073/pnas.1001414107>
- Tzourio-Mazoyer, N., Landeau, B., Papathanassiou, D., Crivello, F., Etard, O., Delcroix, N., Mazoyer, B., Joliot, M., Jan. 2002. Automated anatomical labeling of activations in SPM using a macroscopic anatomical parcellation of the MNI MRI single-subject brain. *NeuroImage* 15 (1), 273–289.
 URL <http://dx.doi.org/10.1006/nimg.2001.0978>
- Van Dijk, K. R., Hedden, T., Venkataraman, A., Evans, K. C., Lazar, S. W., Buckner, R. L., Jan. 2010. Intrinsic functional connectivity as a tool for human

connectomics: theory, properties, and optimization. *Journal of neurophysiology* 103 (1), 297–321.

URL <http://dx.doi.org/10.1152/jn.00783.2009>

Vanhoutte, G., Verhoye, M., der Linden, A. V., May 2006. Changing body temperature affects the $t2^*$ signal in the rat brain and reveals hypothalamic activity. *Magn Reson Med* 55 (5), 1006–1012.

URL <http://dx.doi.org/10.1002/mrm.20861>

Wang, K., Liang, M., Wang, L., Tian, L., Zhang, X., Li, K., Jiang, T., Oct. 2007. Altered functional connectivity in early Alzheimer's disease: a resting-state fMRI study. *Human brain mapping* 28 (10), 967–978.

URL <http://dx.doi.org/10.1002/hbm.20324>

Wang, L., Zang, Y., He, Y., Liang, M., Zhang, X., Tian, L., Wu, T., Jiang, T., Li, K., Jun. 2006. Changes in hippocampal connectivity in the early stages of Alzheimer's disease: evidence from resting state fMRI. *NeuroImage* 31 (2), 496–504.

URL <http://dx.doi.org/10.1016/j.neuroimage.2005.12.033>

Willer, C. J., Li, Y., Abecasis, G. R., Sep. 2010. METAL: fast and efficient meta-analysis of genomewide association scans. *Bioinformatics* 26 (17), 2190–2191.

URL <http://dx.doi.org/10.1093/bioinformatics/btq340>

Yan, C., Liu, D., He, Y., Zou, Q., Zhu, C., Zuo, X., Long, X., Zang, Y., May 2009. Spontaneous Brain Activity in the Default Mode Network Is Sensitive to Different Resting-State Conditions with Limited Cognitive Load. *PLoS ONE* 4 (5), e5743+.

URL <http://dx.doi.org/10.1371/journal.pone.0005743>

Yan, C.-G., Cheung, B., Kelly, C., Colcombe, S., Craddock, R. C., Di Martino, A., Li, Q., Zuo, X.-N., Castellanos, F. X., Milham, M. P., Aug. 2013a. A comprehensive assessment of regional variation in the impact of head micro-movements on functional connectomics. *NeuroImage* 76, 183–201.

URL <http://dx.doi.org/10.1016/j.neuroimage.2013.03.004>

Yan, C.-G. G., Craddock, C. C., Zuo, X.-N. N., Zang, Y.-F. F., Milham, M. P., Oct. 2013b. Standardizing the intrinsic brain: towards robust measurement of inter-individual variation in 1000 functional connectomes. *NeuroImage* 80, 246–262.

URL <http://view.ncbi.nlm.nih.gov/pubmed/23631983>

Yang, H., Long, X.-Y., Yang, Y., Yan, H., Zhu, C.-Z., Zhou, X.-P., Zang, Y.-F., Gong, Q.-Y., May 2007. Amplitude of low frequency fluctuation within visual areas revealed by resting-state functional mri. *Neuroimage* 36 (1), 144–152.

URL <http://dx.doi.org/10.1016/j.neuroimage.2007.01.054>

- Zhang, H., Wang, S., Xing, J., Liu, B., Ma, Z., Yang, M., Zhang, Z., Teng, G., Jan. 2009. Detection of PCC functional connectivity characteristics in resting-state fMRI in mild Alzheimer's disease. *Behavioural Brain Research* 197 (1), 103–108.
URL <http://dx.doi.org/10.1016/j.bbr.2008.08.012>
- Zhang, H., Zuo, X.-N., Ma, S.-Y., Zang, Y.-F., Milham, M. P., Zhu, C.-Z., Mar. 2010. Subject Order-Independent Group ICA (SOI-GICA) for Functional MRI Data Analysis. *NeuroImage*.
URL <http://dx.doi.org/10.1016/j.neuroimage.2010.03.039>
- Zijdenbos, A. P., Forghani, R., Evans, A. C., Oct. 2002. Automatic "pipeline" analysis of 3-D MRI data for clinical trials: application to multiple sclerosis. *IEEE Transactions on Medical Imaging* 21 (10), 1280–1291.
URL <http://dx.doi.org/10.1109/TMI.2002.806283>
- Zuo, X.-N., Xu, T., Jiang, L., Yang, Z., Cao, X.-Y., He, Y., Zang, Y.-F., Castellanos, F. X., Milham, M. P., Oct. 2012. Toward reliable characterization of functional homogeneity in the human brain: Preprocessing, scan duration, imaging resolution and computational space. *NeuroImage*.
URL <http://dx.doi.org/10.1016/j.neuroimage.2012.10.017>

6. Figure Legends

7. Table Legend

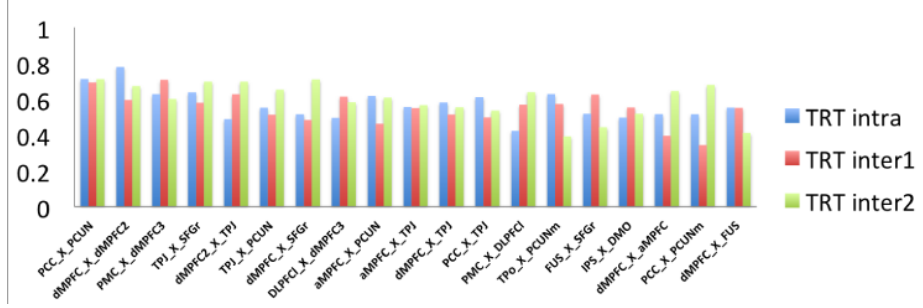


Figure 1: ICC scores for pairs of connections passing the > 0.5 threshold on the NYU-TRT dataset.

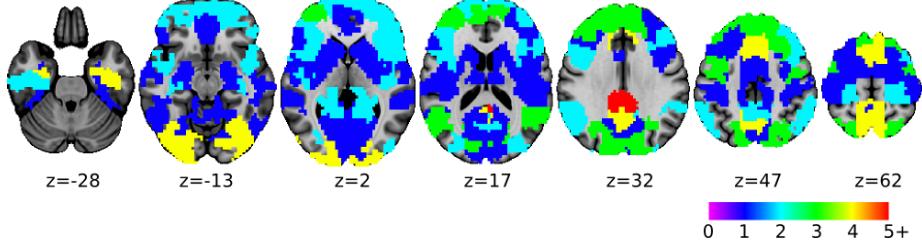


Figure 2: Frequency of reported regions showing functional differences based on a literature review of 6 papers.

Network	Label	Name	Cambridge100
Default-mode network	PCC	posterior cingulate cortex	1
	dMPFC	dorsomedial prefrontal cortex	12
	dMPFC2	dorsomedial prefrontal cortex	46
	aMPFC	anterior medial prefrontal cortex	42
	IPL	inferior parietal lobule	49
	PCUN	precuneus	53
	MTL	medial temporal lobe	39
Visual network	FUS	fusiformgyrus	71
Dorsal attentional	PCUMM	precuneus (motor)	94
Cingulo-opercular network	dMPFC3	dorsomedial prefrontal cortex	90

Table 1: Regions selected in the literature review, the region number correspond to the number in the Cambridge 100 partition.

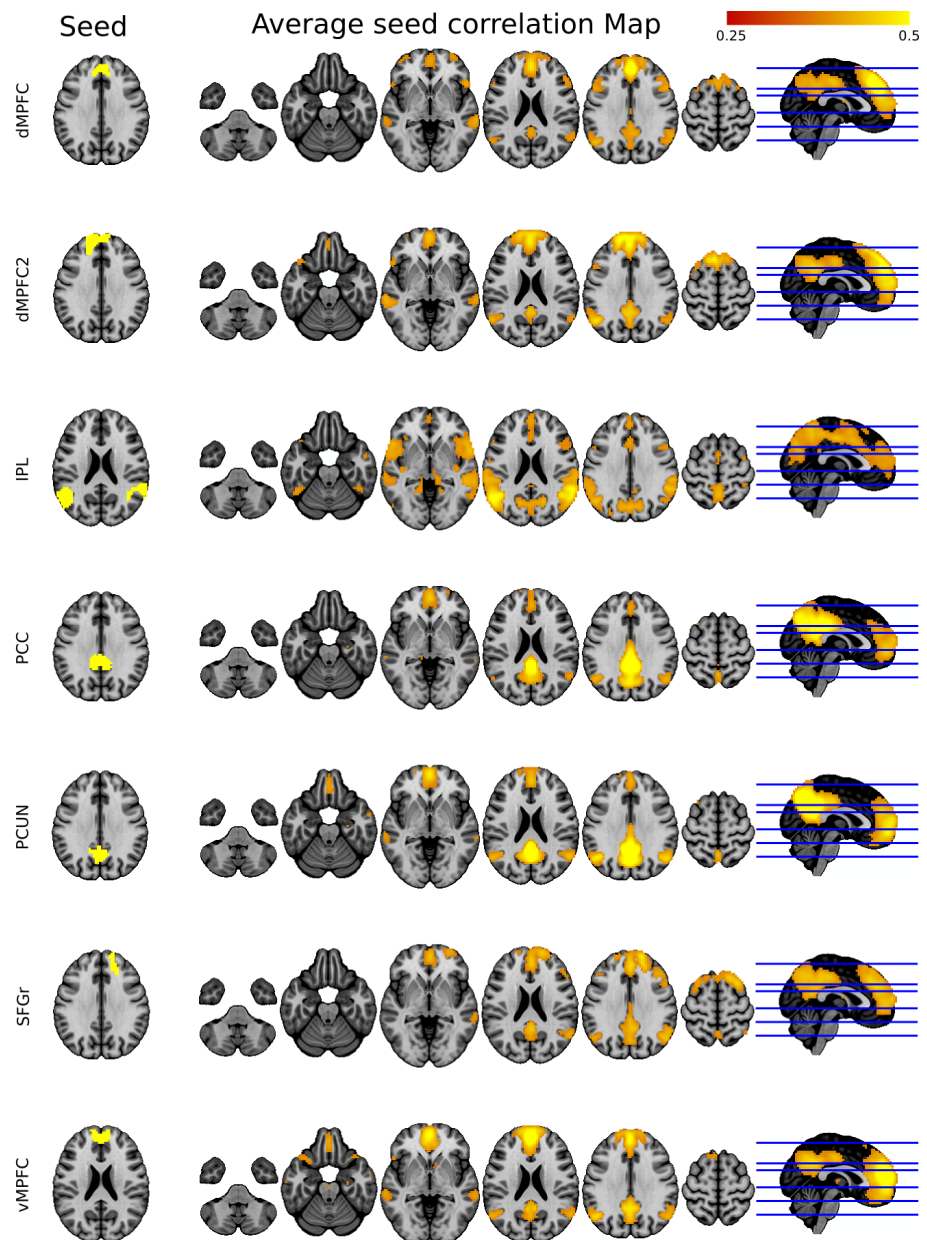


Figure 3: Selected nodes inside the DMN who passed the TRT selection.

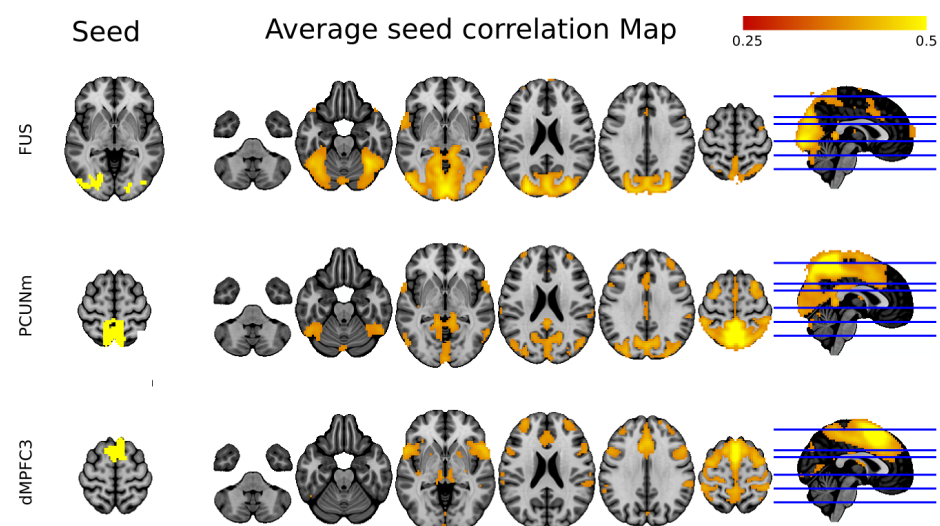


Figure 4: Selected nodes outside the DMN who passed the TRT selection.

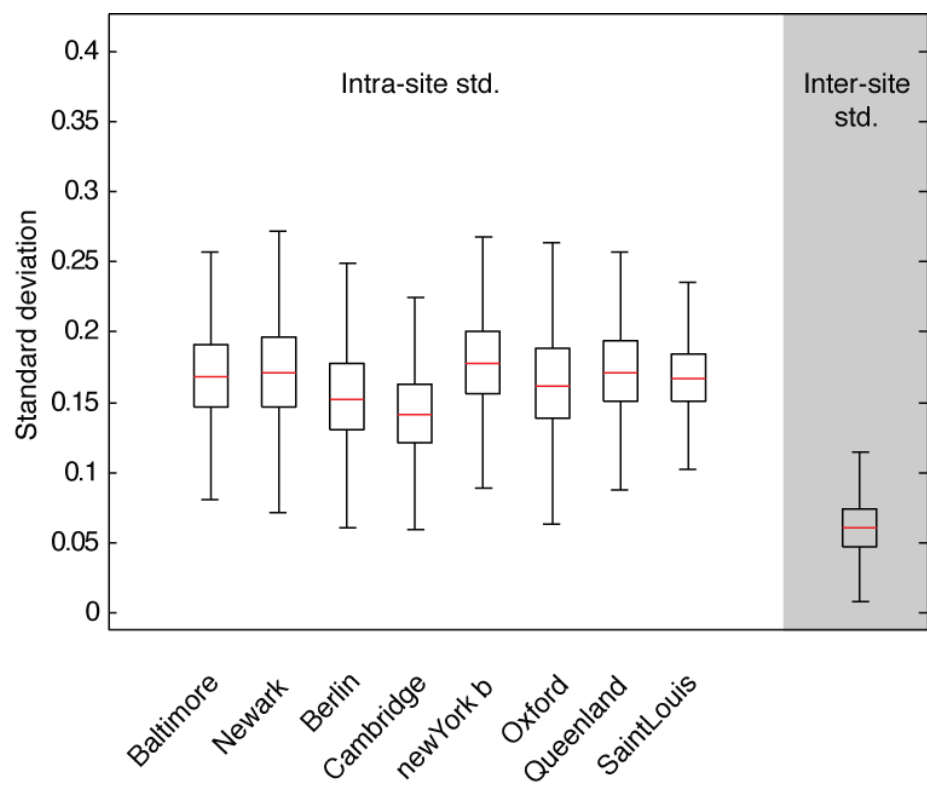


Figure 5: Distribution of intra-site (between-subject) standard deviation vs. inter-site (between-site) standard deviation, based on the standard deviation of the connectivity matrices from 8 sites from the 1000 functional connectome dataset.

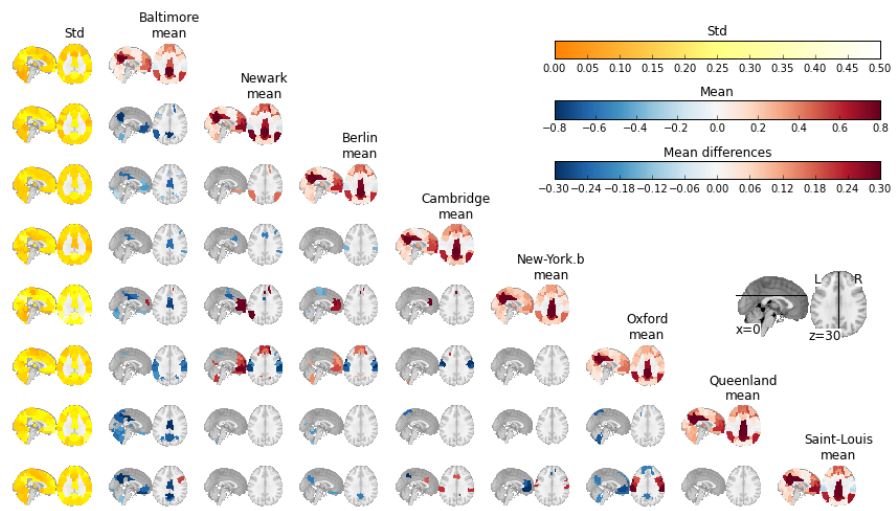


Figure 6: Functional connectivity maps of the default-mode network at multiple sites. The average connectivity map for 4 sites (Baltimore, Cambridge, Newark and New-York.b at 3T) are presented on the diagonal (left). The standard deviation across subjects and within site is presented next to it (diagonal squares, right part). Each off-diagonal block represent the absolute difference between the average functional connectivity maps between two sites (called the inter-site bias).

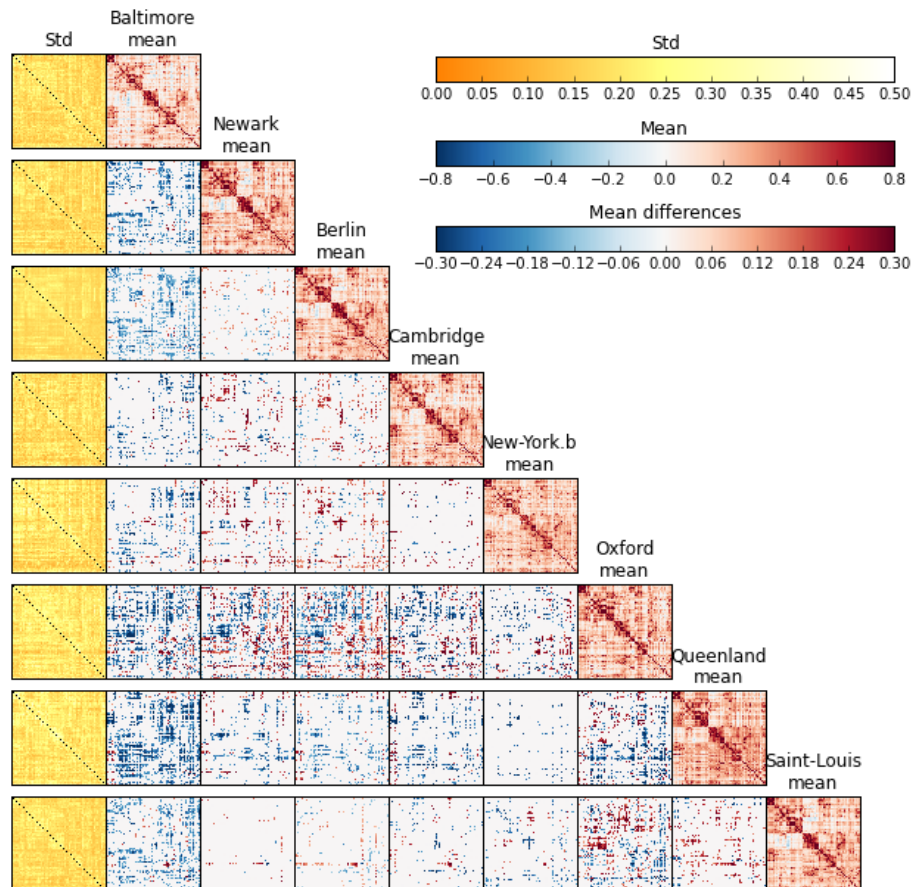


Figure 7: Functional connectome for multiple sites. The average connectome of 7 sites (Baltimore, Cambridge, Newark and New-Yorkb, Oxford, Queenland, SaintLouis at 3T) are presented on the diagonal (left). The standard deviation across subjects and within site is presented next to it (diagonal squares, right part). Each off-diagonal block represent the absolute difference between the average functional connectivity maps between two sites (called the inter-site bias).

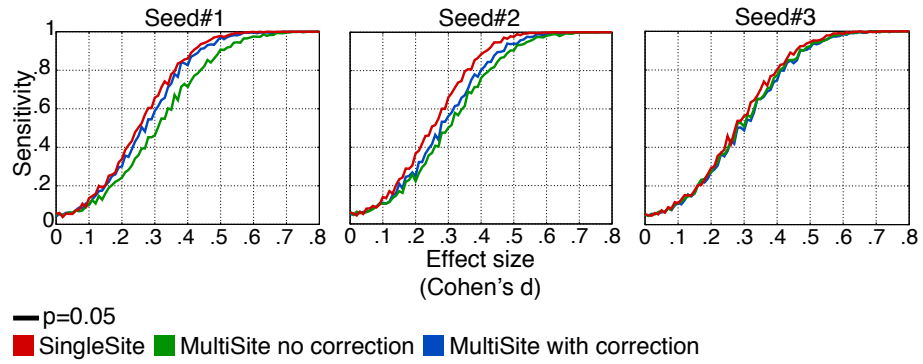


Figure 8: Power analysis for a resting-state fMRI study. A Monte-Carlo simulation was implemented to evaluate the power of a resting-state multi-site study, based on real values of three connections in the default-mode network PCC/MFC, rHIP/vMFC and IIPC-rDLPFC. For each site and each sample, half of the subjects were randomly assigned to a 'treatment' group. For the subjects in this group, a value was added to achieve a given relative effect size (Cohen's d , i.e. the mean of the two groups divided by the standard deviation of all sites). The significance of the difference between the control and 'treatment' group was assessed by a t -test in a linear model, including covariates to model site-specific bias. The study was repeated for various effect sizes (0 to 0.8 with a step of 0.01) at a threshold of 0.05 on the p -value in the t -test. For a p of 0.05, a statistical power of 0. 95 can be achieved for as low as a 0.47 effect size. The simulation was based on a scenario with 8 sites and 385 subjects, and no homogenization of acquisition protocol whatsoever. The multi-site (with and without correction) is based on 187 subjects from 7 sites and the SingleSite is based on one site of 198 subjects.

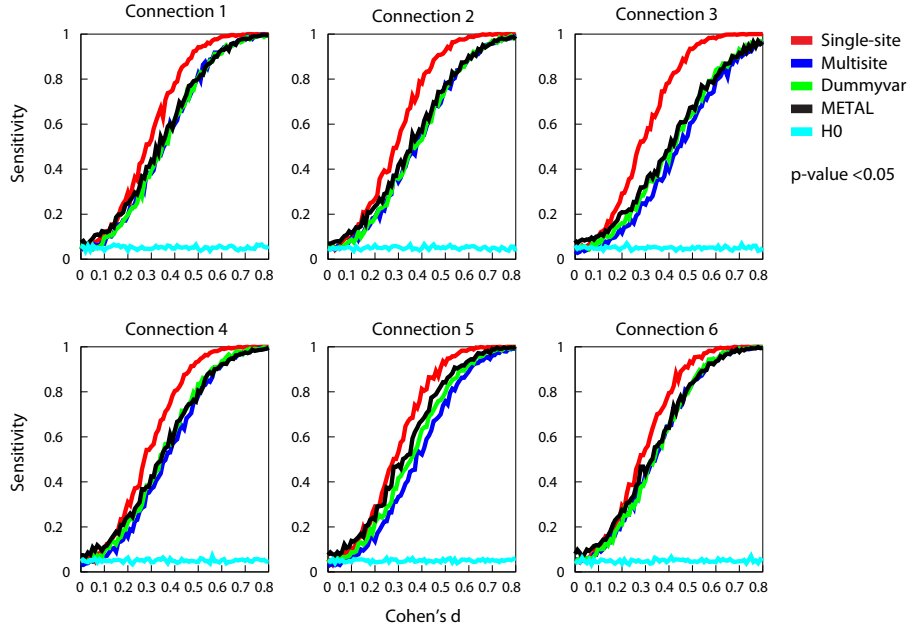


Figure 9: Power analysis for a resting-state fMRI study. A Monte-Carlo simulation was implemented to evaluate the power of a resting-state multi-site study. For each site and each sample, half of the subjects were randomly assigned to a 'treatment' group. For the subjects in this group, a value was added to achieve a given relative effect size (Cohen's d , i.e. the mean of the two groups divided by the standard deviation of all sites). The significance of the difference between the control and 'treatment' group was assessed by a t -test in a linear model. To correct for site-specific bias two correction are presented the dummy variables and METAL. The study was repeated for various effect sizes (0 to 0.8 with a step of 0.01) at a threshold of 0.05 on the p-value in the t -test. The simulation was based on a scenario with 8 sites and 385 subjects, and no homogenization of acquisition protocol whatsoever. The multi-site (with and without correction) is based on 187 subjects from 7 sites and the Single-site is based on one site of 198 subjects.

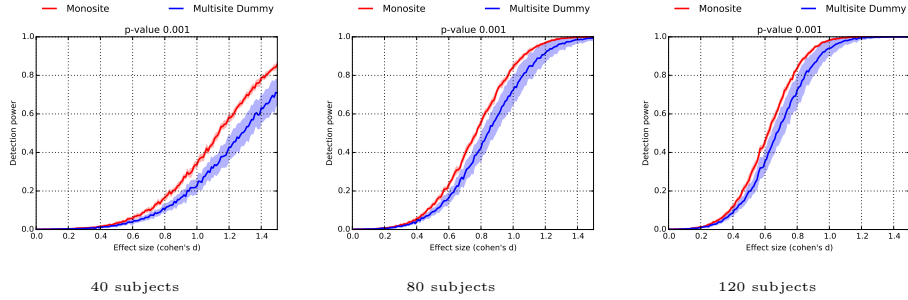


Figure 10: Simulation on real data of the detection power of two groups balanced 50%-50% between 7 sites. All plot show four scenario, one monosite, 7 sites with no correction for differences in variability between sites, 7 sites with correction for multisite differences using dummy variables and 7 sites with correction for multisite differences using METAL weighted average. Each plot show the detection power in function of the effect size for 3 different sample size 40, 80 and 120 subjects in total.

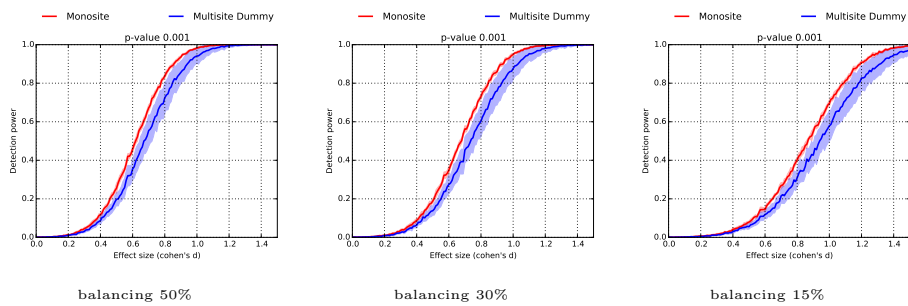


Figure 11: Simulation on real data of the detection power of two groups for a total of 120 subject between 7 sites. All plot show four scenario, one monosite, 7 sites with no correction for differences in variability between sites, 7 sites with correction for multisite differences using dummy variables and 7 sites with correction for multisite differences using METAL weighted average.

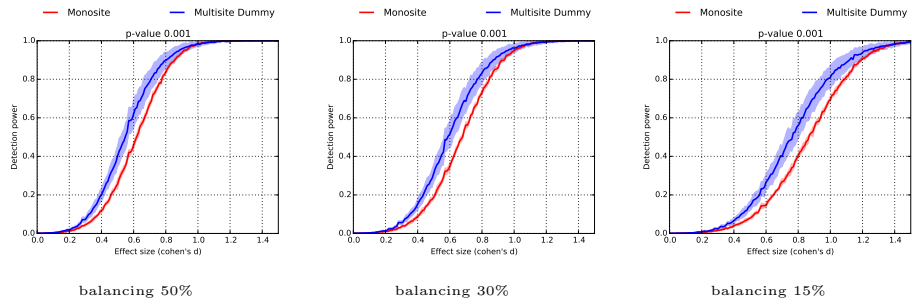


Figure 12: Simulation on real data of the detection power of two groups for a total of 120 subject between 7 sites. All plot show four scenario, one monosite, 7 sites with no correction for differences in variability between sites, 7 sites with correction for multisite differences using dummy variables and 7 sites with correction for multisite differences using METAL weighted average.

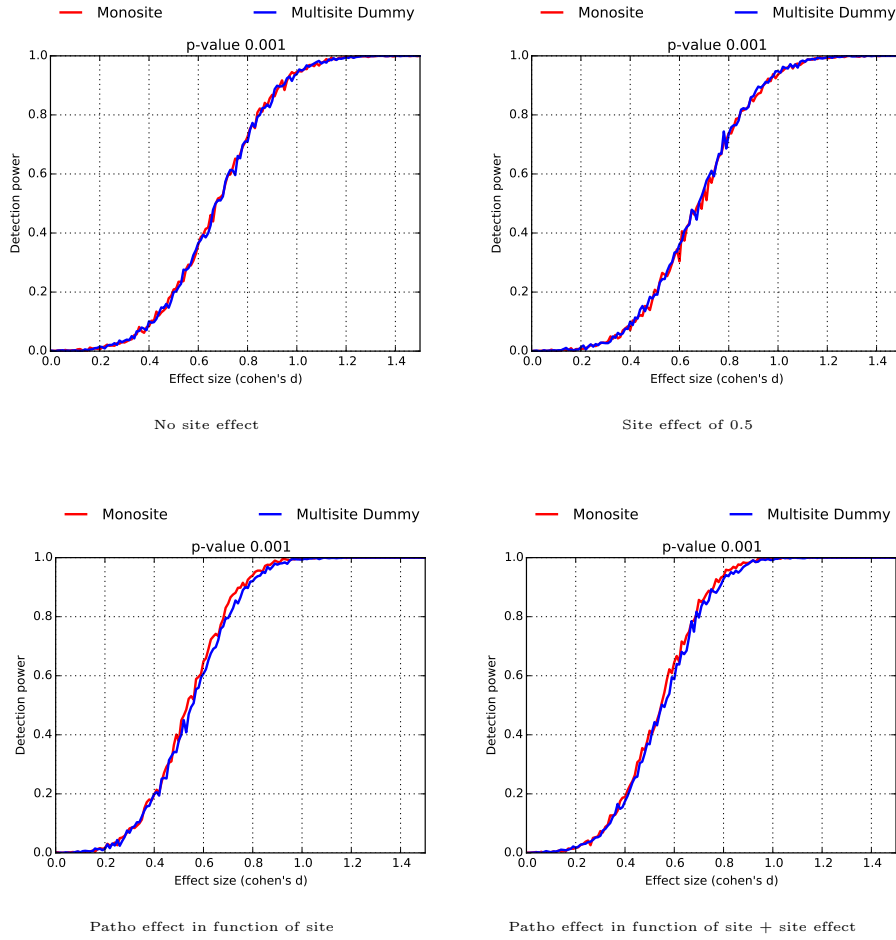


Figure 13: Simulation of the detection power of two groups balanced 50%-50% between two sites. All plot show four scenario, one monosite, two sites with no correction for differences in variability between sites, two sites with correction for multisite differences using dummy variables and two sites with correction for multisite differences using METAL weighted average. The plots show the detection power when the variability is greater in one side then the other for the pathology group (twice the reference variability in one site and half the reference variability in the other one)

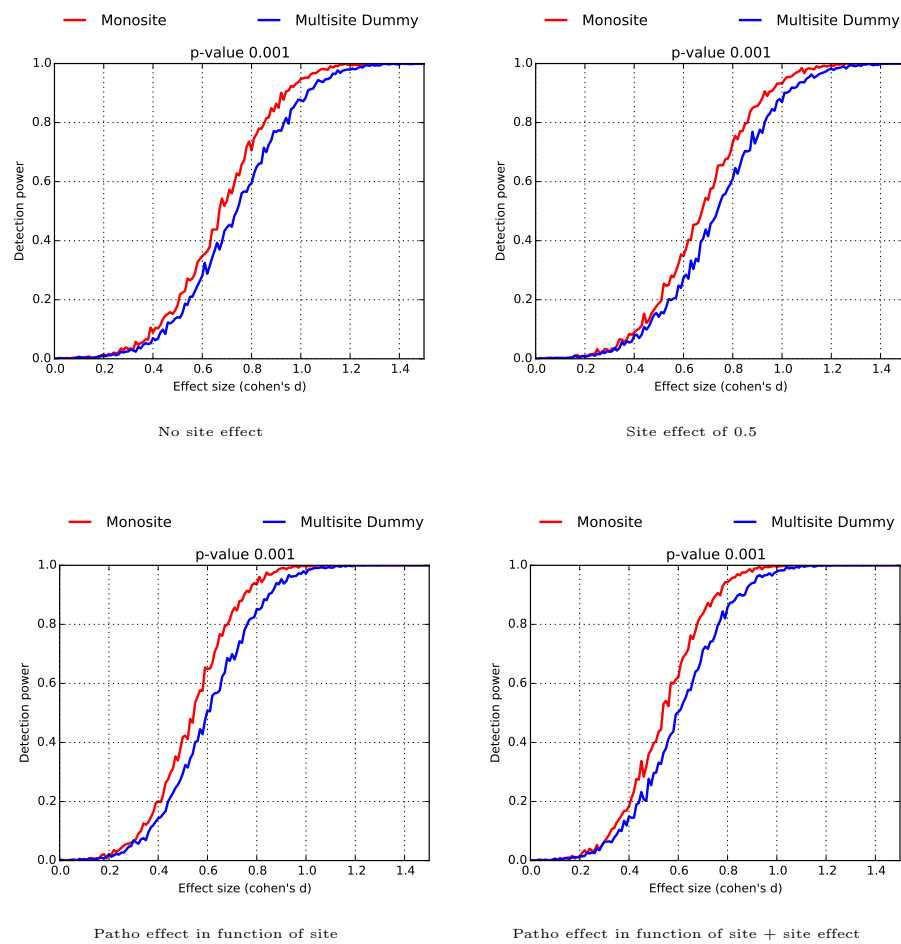


Figure 14: balance 70%-30%

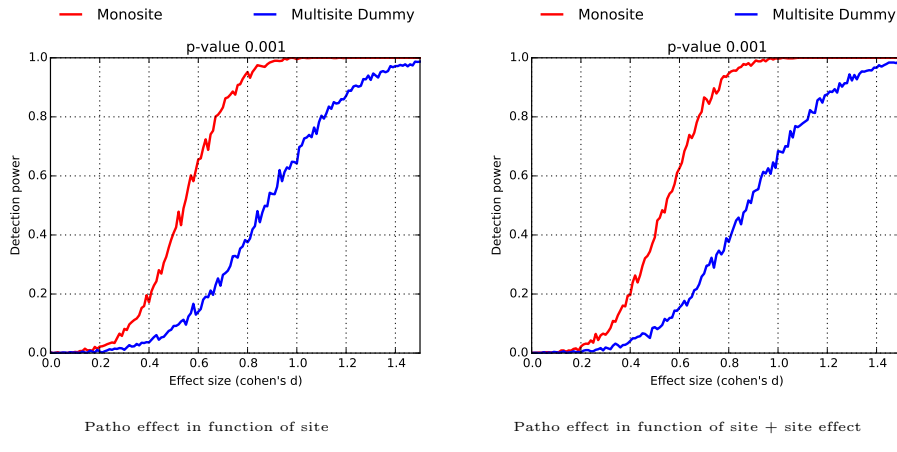


Figure 15: Small and big site, balance 50%-50%

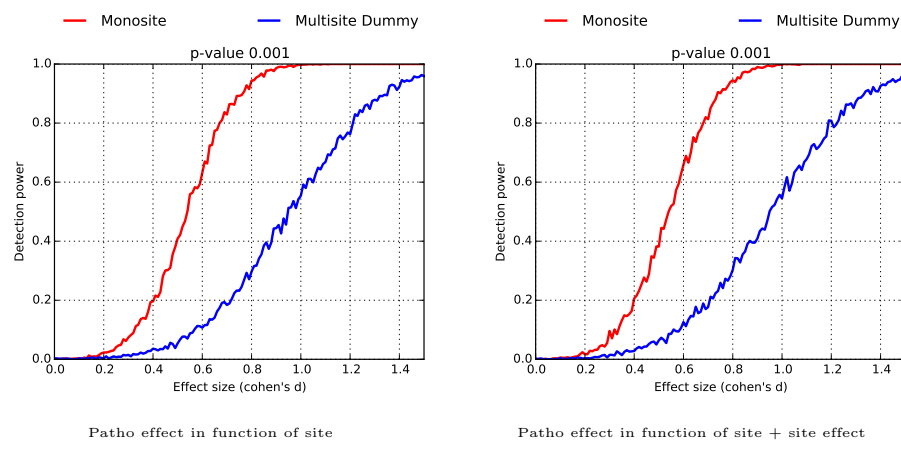


Figure 16: Small and big site, balance 70%-30%

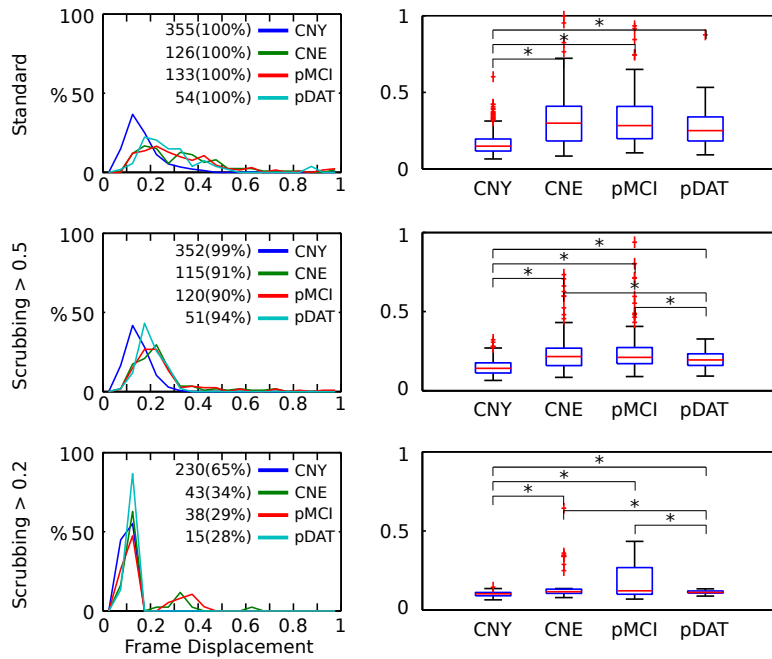


Figure 17: Distribution of the frame displacement (FD) for 3 groups (CNE, pMCI, pDAT) when scrubbing is applied at various levels (no scrubbing, scrubbing of $FD > 0.5$ and scrubbing of $FD > 0.2$). The figures on the right depict a boxplot representation of the distributions with their associated statistical differences t -test (marked with a * for a $p < 0.05$).

Supplementary Material – Feasibility of multi-centric fMRI connectivity studies of Alzheimer's disease

Submitted to Neuroimage.

C. Dansereau^{1,2}, C. Risterucci³, E. Merlo Pich³, D. Arnold⁴, P. Bellec^{1,2}

¹Functional Neuroimaging Unit, Centre de Recherche de l'Institut Universitaire de Gérontologie et de Médecine de Montréal

²Department of Computer Science and Operations Research, University of Montréal, Montreal, Quebec, Canada

³F. Hoffmann-La Roche Ltd., Basel, Switzerland

⁴NeuroRx, Montreal, Quebec, Canada

For all questions regarding the paper, please address correspondence to Pierre Bellec, CRIUGM, 4545 Queen Mary, Montreal, QC, H3W 1W5, Canada. Email: pierre.bellec (at) criugm.qc.ca.

Literature review: Alzheimers disease and resting-state fMRI

- Zhang et al. (2009) used functional connectivity maps with a seed in the posterior cingulate cortex (PCC) to explore the differences between a group of elderly cognitively normal subjects (CNE, n=16) and patients with a mild dementia of the Alzheimers type (DAT, n=18).
- Zhang et al. (2010) generalized the Zhang et al. (2009) study with CNE (n=16) and a larger group of patients with DAT (n=46). Patients were separated in three groups (mild, moderate, severe DAT), and each group of patients was contrasted against the CNE.
- Wang et al. (2006) used functional connectivity maps with a seed in the hippocampi to explore the differences between a group of CNE (n=13) and patients with a mild DAT (n=13). All results included in the meta-analysis are from Table 2, seeded in the right hippocampus. Seeds were manually delineated on an individual basis.
- Wang et al. (2007) used functional connectivity maps with a seed in the posterior cingulate cortex (PCC) as well as full brain point-to-point correlations (based on an AAL parcellation) to explore the differences between a group of elderly cognitively normal subjects (CNE, n=14) and patients with a very mild to mild dementia of the Alzheimers type (DAT, n=14). Only the results based on the PCC seed were included in the meta-analysis.
- Goveas et al. (2011) used functional connectivity maps with a seed in the hippocampi to explore the differences between a group of elderly cognitively normal subjects (CNE, n=18) and patients with a mild dementia of

the Alzheimers type (DAT, n=14) before and after donepezil treatment. Seeds were manually delineated on an individual basis, before and after treatment.

- Damoiseaux et al. (2012) used dual-regression independent component analysis to explore longitudinal differences between a group of CNE (n=18) and patients with DAT (n=21). All results included in the meta-analysis are from Table 3 (differences at baseline) and Table 4 (interaction with time). The authors used three components representing the Anterior DMN, Ventral DMN and Posterior DMN.

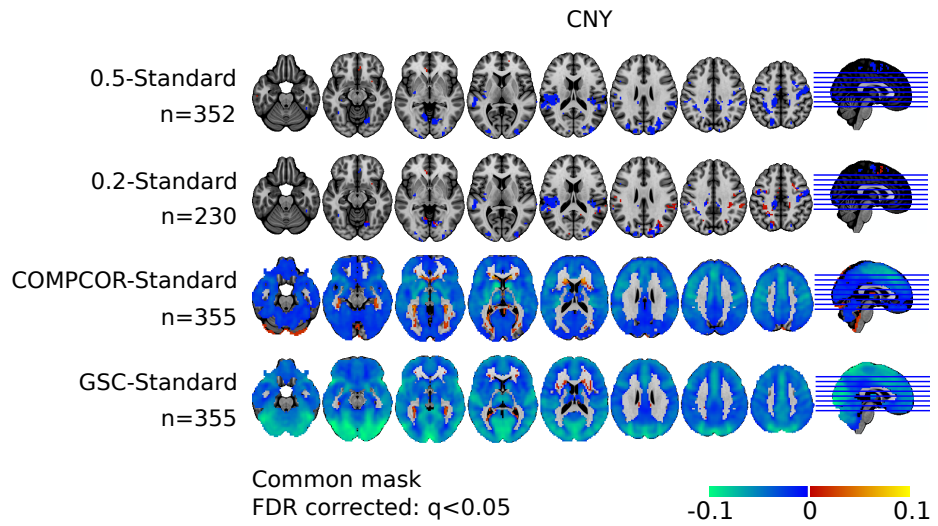


Figure S1: Differences in functional connectivity for the default mode network (seed in the PCC). Differences in connectivity between all the CNY with scrubbing ($FD > 0.5$ and $FD > 0.2$), CompCor, and GSC. The mask used depict only significant result of the t -test (FDR correction $q < 0.05$) only the two scrubbing procedures use the union of there respective mask (common mask).

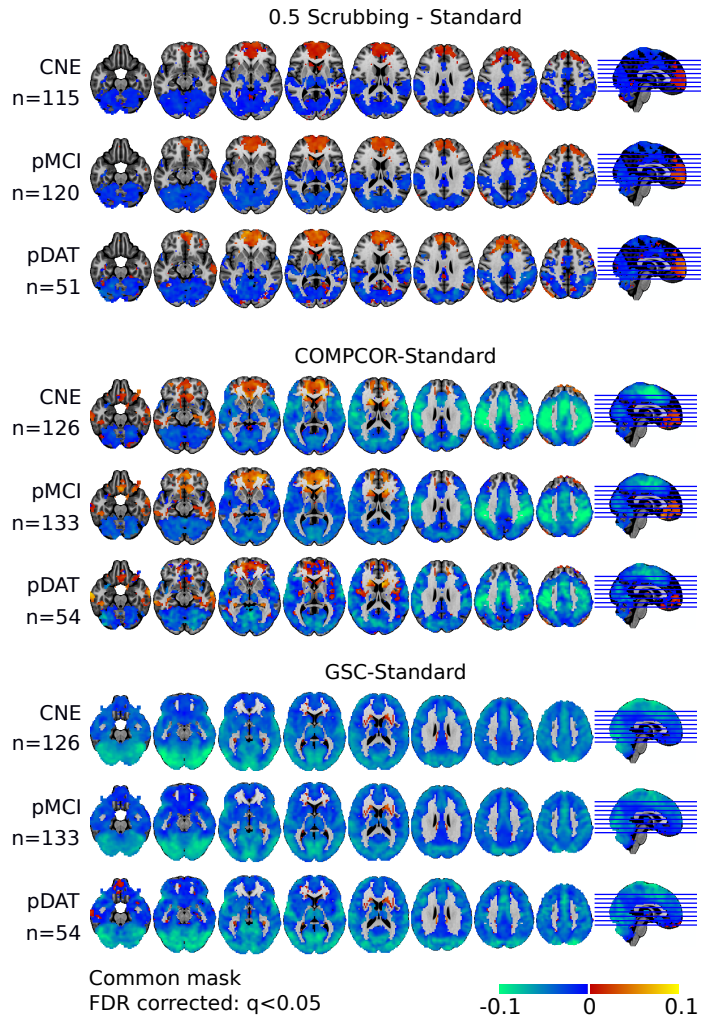


Figure S2: Differences in functional connectivity for the default mode network (seed in the PCC). Differences in connectivity for each group (CNE, pMCI, pDAT) compared to baseline (standard preprocessing) with and without scrubbing ($FD > 0.5$ and $FD > 0.2$) (FDR correction $q < 0.05$) for all voxels showing a significant effect in at least one of the contrast.